04

Gas targets for point-like source of vacuum and extreme ultraviolet radiation sustained by focused electromagnetic radiation

© A.V. Sidorov, A.P. Veselov, A.V. Vodopyanov, A.A. Murzanev, A.N. Stepanov

Federal Research Center A.V. Gaponov-Grekhov Institute of Applied Physics of the Russian Academy of Sciences,
603950 Nizhny Novgorod, Russia
e-mail: alexsv@ipfran.ru

Received April 23, 2024
Revised April 23, 2024
Accepted April 23, 2024

In this work, an experimental study of various gas targets for a point-like plasma source based on a discharge in a non-uniform gas flow was carried out. As a result of the experiments, it was possible to observe the structures of injected jets for different targets with different gas inlet holes. It has been demonstrated that with a significant decrease in the pressure of the background gas, the jet practically collapses and the gas is injected evenly in all directions.

Keywords: Discharge in a non-uniform gas flow, extreme ultraviolet radiation, gas jet interferometry.

DOI: 10.61011/TP.2024.07.58796.135-24

Introduction

Unprecedented microelectronic development that has been observed over the previous 50 years is primarily attributed to continuously decreasing minimum sizes of integrated-circuit elements. For some time, the progress in this area was facilitated by photolithography improvements using a part of visible band, ultraviolet and near vacuum-ultraviolet bands of electromagnetic radiation spectrum. However, the capabilities of optical schemes are limited by the diffraction limit and the maximum resolution, according to the Rayleigh criterion, is proportional to the wavelength of the radiation. Therefore, it seems logical to move deeper into the vacuum-ultraviolet range — to extreme ultraviolet radiation. Difficulties arising in this process are primarily caused by the absence of transparent materials for this wavelength bandwidth and a need for high-performance radiation sources within it.

The absence of necessary optically transparent materials forces transition, in particular, to reflective optics which in turn results in evident reduction of the numerical lens aperture and corresponding resolution drop.

The foregoing places emphasis on wave processes in the extreme ultraviolet (EUV) band where a visible progress has been achieved recently in reflective optical elements and high-performance radiation sources. Creation of mirrors having quite high reflectance in the EUV band might be one of the key aspects. For this, multilayer Bragg coating on an atomically smooth surface of a bulk substrate with a predefined curvature is used. It has been believed until recently that systems on the basis of Mo/Si layers are a single mirror option for the EUV lithography because the highest EUV radiation reflectances about 74% within 13.5 ± 1 nm) have been achieved for them.

Laser-induced plasma on solid tin target has been used over the last 10 years in the industrial EUV lithography for generation of the useful radiation with wavelength near $\lambda = 13.5$ nm. Nevertheless, introduction of EUV lithography at $\lambda = 13.5$ nm into large-scale commercial manufacturing is still delayed (see, for example, [1]) due to insufficient intensity of the useful radiation and formidable obstacles associated with large micron-size fragmentation fluxes that contaminate the optical system resulting in its quick failure. Their contact with the mask is particularly dangerous and results in reproduction of defective structures in ICs. Invention and utilization of numerous special protection techniques for the optical path did not provide a radical problem solution. This forced to use supersonic gas jets of a heavy inert gas — xenon. Inert gas used as a target generally solves the contamination problem. The most dangerous position in the source is taken by the collector mirror placed in the maximum vicinity to the convertor target. In case of a xenon gas jet, some corrosion is still recorded only on the collector mirror due to bombardment by high-energy ions and inert gas atoms that limits the life. However, it is more important that the conversion ratio has to be compromised for the sake of contamination control because the xenon radiation efficiency at 13.5 nm is much lower than that of tin. Therefore, the concept of using the tin plasma as a source of EUV radiation for the projection lithography has become prevailing at a certain point.

Commercially available 13.5 nm sources are already manufactured by ASML, a European company, and similar research is also carried out in Russia [2] and China [3]. As an alternative to 13.5 nm, an idea was put forth to switch the EUV lithography to $\lambda = 11.2$ nm with a xenon gas target used in the radiation source [4]. As mentioned above, a xenon gas target source was first proposed for the EUV lithography with $\lambda = 13.5$ nm as early as in the 1990s [5],

however, its radiation power was too low due to the low ratio of conversion of the heating radiation into the EUV radiation at 13.5 nm, and it was abandoned.

According to the authors of [4], the idea proposed by them will be successful, because the intensity at $\lambda = 11.2$ nm in the xenon radiation band may be 4 to 5 and more times higher than the intensity at $\lambda = 13.5$ nm. Nevertheless, for the reasons mentioned above, the $\lambda = 11.2$ nm lithography has been held impossible until recently due to the absence of effective interference mirrors for this wavelength. But at this point, the Institute for Physics of Microstructures of the Russian Academy of Sciences has created the world's first Mo/Be mirror prototypes suitable for operation at $\lambda = 11.2$ nm [6]. And the Ru/Be-based mirrors might be even more effective [4]. All this breathed a new life into the concept of a point source of EUV radiation for the projection lithography based on multicharged xenon ion plasma.

Several research teams conducted the experiments to examine discharge on gas targets [5]. The experiments also were aimed at the development of an extreme ultraviolet radiation source [7,8]. Summing up, it should be noted that the efficiency of laser radiation energy conversion is equal to units of percent or fractions of percent. And it has been theoretically and experimentally shown that in case of, for example, tin plasma, reduction of the IR laser radiation frequency from 300 to 30 THz (or increase in the wavelength from 1 to 10 μm) results in improved matching and, therefore, in increased performance of the extreme ultraviolet source [9]. Further wavelength increase/frequency decrease results in transition to the THz frequency band.

According to the guidelines of the „International Telecommunication Union“ (ITU), the terahertz frequency range includes a spectrum segment from 300 GHz to 3 THz. However, this range is often extended to 100 GHz–10 THz. For a long time, this range has seemed too short-wavelength for electrovacuum sources of coherent electromagnetic radiation and too long-wavelength for quantum generators and, thus, beyond the reach of researchers. This is, in particular, applicable to the experiments for generation and maintenance of plasma by the terahertz electromagnetic radiation because this requires a relatively high radiation power (kW level and higher).

In the case of electrovacuum devices, a natural solution to the problems with short wavelengths is to move to electrovacuum devices that do not have slowing systems (i.e., operate with „fast“ waves), such as free-electron lasers and gyrotrons. It is their evolution (primarily the growing radiation power) that has recently ensured a considerable progress in the research of gas discharge generated and maintained by the THz radiation [10].

In terms of a point source of extreme ultraviolet radiation, transition from the IR to THz frequency range of the plasma-heating electromagnetic radiation may turn to be even more beneficial because the plasma concentration typical for the THz discharge (10^{16}–10^{17} cm^{-3}) is better for the EUV radiation [11] and matching between the point plasma the size of which equals to several hundred microns and the electromagnetic radiation [12]. And it has been experimentally shown for the first time that transition to frequencies of 1–3 THz [13] is required to improve the degree of conversion to EUV. Investigations of a point discharge generated in a non-uniform gas flux by 1 THz and 2.3 THz radiation are currently performed by joint efforts of research teams from the Institute of Applied Physics of the Russian Academy of Sciences and the Institute of Nuclear Physics of Siberian Branch of the Russian Academy of Sciences [14,15].

The main idea in generation of the point discharge plasma in a non-uniform gas flux is that the pressurized (about several bar) gas is supplied to the evacuated discharge chamber. Gas admission and evacuation rate control is used to achieve a very non-uniform gas pressure profile in the discharge chamber. Owing to this, on the one hand, breakdown conditions are provided only in a limited area near the gas admission opening and discharge propagation towards the heating radiation is prevented even in case of quite long pulses (more than 100 ns). And on the other hand, low background gas pressure in the discharge chamber ensures conditions for propagation without absorption even for the EUV radiation.

Thus, a so-called gas target is one of the key elements of this EUV source and ensures the required gas pressure profile in the discharge chamber. On the one hand, it shall, as mentioned above, ensure an adequate density of working gas particles for plasma generation and, on the other hand, it shall ensure evacuation of the background gas volume to a pressure at the forevacuum level and, finally, provide the best matching between the electromagnetic radiation and discharge plasma.

Another distinguishing feature shall be also emphasized, though it is typical for IR radiation generating plasma in the gas jet, rather than for the THz range. In particular, for 1 μm radiation.

In this case, the xenon-target laser-plasma source is examined with point beam focusing (with a focal spot diameter equal to dozens of micrometers) of laser to the most dense part of the gas-jet target near its center line. Such configuration is optimum for laser-induced breakdown followed by plasma heating, but in this case the EUV-radiating plasma core is surrounded by a peripheral shell consisting of neutral atoms and relatively low ionized xenon ions where photoionization absorption of the EUV radiation at both wavelengths (11.2 and 13.5 nm) exceeds 90%. This circumstance was addressed in the earliest studies. Attempts were made to reduce this absorption, however, the achieved benefit in the EUV radiation yield was not high (maximum 2.5 times as high). New methods to overcome this difficulty are currently addressed (see, for example, [16] and references therein). An effective method to control the EUV radiation absorption by gas is formation of a gas jet target such as to increase the density in its center and reduce the peripheral density. This may have a positive effect on the increase in the „point-like“ nature of discharge. Certainly, a

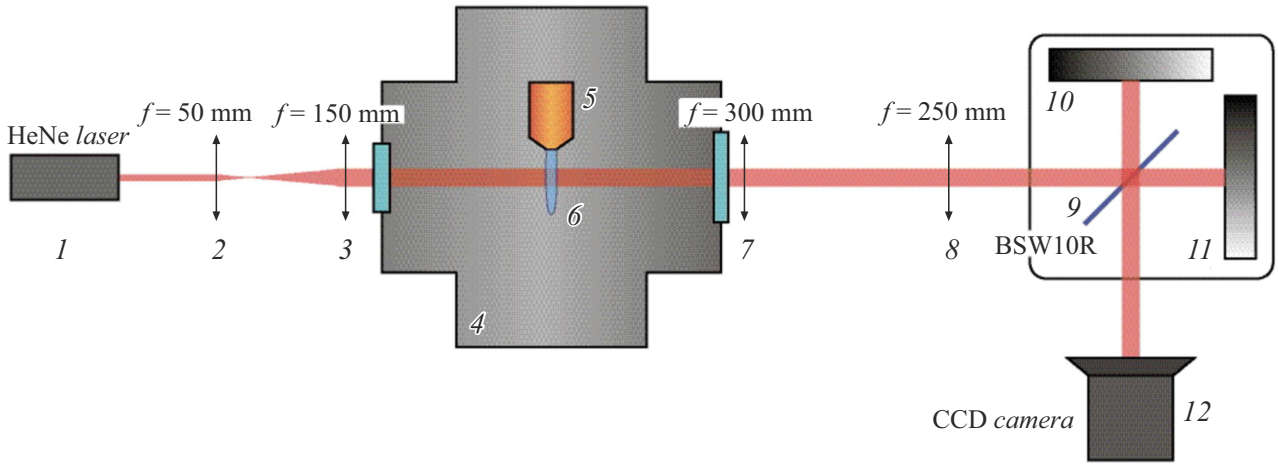

Figure 1. Experiment setup for interferometric measurements of gas jets. *1* — He-Ne laser; *2, 3* — laser beam transfer lens system; *4* — vacuum chamber; *5* — gas target; *6* — gas jet; *7, 8* — image transfer system; *9–11* — the Michelson interferometer, *12* — CCD camera.

significant help in the optimization of the source/gas target may be provided by a calculated pre-experimental analysis based on the numerical simulation of the jet. Nevertheless, even in case of successful simulation with high accuracy of calculations, behavior of the really prepared target may somewhat differ from the calculations which may be caused by the accuracy of preparation of the gas target. In this case, post-fabrication testing of gas targets involving the analysis of behavior of the gas jet flowing from the target plays an important role.

This study describes an example of experimental investigation of various gas targets for a point plasma source based on a non-uniform gas flux discharge. The structure of the gas jet flowing from the admission opening was examined using the Michelson-type laser interferometer. This interferometer is used to track the refraction index variation on the laser beam path against the surrounding background. The measurements were based on the difference in the refraction indices of the admitted heavy inert gas jet and the background gas in the discharge chamber at various pressures up to the prevacuum pressure.

1. Experimental setup

Gas targets were tested using an evacuated vacuum chamber in the form of a six-pass cross with CF 160 flanges. The chamber was evacuated using a prevacuum pump with a maximum pumping rate of 3 l/s. The vacuum chamber was outfitted with a gas admission system to admit the working gas both through the gas target and directly into the chamber bypassing the target. The admitted gas jet was tested through the oppositely facing optical flanges with built-in windows whose diameters were sufficient to pass the test laser beam.

The parallel He-Ne laser beam *1* ($\lambda = 632.8$ nm) using two lenses with focal distances of 50 mm (*2*) and 150 mm (*3*), respectively, was directed to vacuum chamber *4* through the optical inlet flange (Figure 1). To ensure uniform exposure of the test area with a typical size of about 1 mm, 3 x magnification of the laser beam was provided. The laser beam passed through the vacuum chamber. The gas target *5* was placed inside the chamber in such a manner that the beam touched the target metal and the generated gas jet *6* took approximately 1/4 of the beam cross-section.

The image transfer system consisted of two lenses with focal distances of 25 cm (*7*) and 30 cm (*8*) to produce the image of an object on the digital CCD chamber (*12*) with a reduction ratio of 1.2. SDU-285 „Spetsteletekhnika“ camera was used to provide imaging on the camera matrix with a scaling ratio of 5.3 μm/px.

Phase incursion induced by the gas target placed on its path was measured by the Michelson interferometer consisting of two aluminium mirrors 50 mm in diameter (*10, 11*) and BSW11R (*9*) („Thorlabs“) beam-splitting plate. In our case, the interferometer was set in such a manner that beam interference occurred when one part of the beam, carrying the data on phase incursion on the propagation path due to the gas target, overlaps the other reference part of the beam the phase in which was not excited and was almost flat. The fringe pattern occurs when two beams separated in the interferometer are overlapped on the digital camera matrix. The camera that recorded the interference pattern was placed as close as possible to the interferometer in order to achieve a steep beam convergence angle and, consequently, thin lines in the interference pattern and smaller line spacing. On the other hand, it was necessary to ensure that at least 7 pixels of the camera matrix, i.e. approx. 37 μm, fall within the distance δ between the fringe pattern peaks. Since $\delta \sim \lambda(b/a)$, where λ is the laser wavelength, b is the distance between the interferometer and CCD camera matrix, a is the center-to-center distance between the probe and reference beams. Since the latter is defined by the test area dimensions (about 1 mm), b

shall be more than 7 cm, which in our case was satisfied more than enough because b was about 20 cm. Thus, we achieved quite narrow lines on the interference pattern and at the same time an adequate resolution of these lines by the CCD camera.

2. Experimental results

The optical system was set with image definition control of the needle installed in plane with the gas jet opposite to the nozzle. The „dark-field“ method was used as an additional simple validation of the optical system setting. A point of a needle was placed in the focal waist between the image transfer lenses. The fine-focused light of the He-Ne laser was fully overlapped, while the scattered light caused by scattering at the object edge near the gas jet was diverging and, therefore, was not overlapped by the point of the needle. Thus, light object outlines in the vicinity of the gas jet and much less bright, though distinguishable above the background level, jet image were observed on the camera matrix. The dark-field method is suitable for visualization of small-scale and phase objects as an auxiliary means of setting the optical system, but any measurements or assessment of the concentration of neutral gas atoms using this method do not seem possible.

The dark-field jet analysis has shown that after admission activation, almost steady-state gas flow through the nozzle was established almost immediately and no jet perturbation behavior was observed. Therefore, for fringe pattern recording, exposure time for making one interference pattern frame was equal to 800 μs.

For the experiment, it was possible to vary both the background pressure in the vacuum chamber and the pressure in the gas admission tube through the target. To restore the phase incursion, two images were made for each pressure without and with gas jet. Thus, phase incursions caused by the geometrical deformations of the chamber walls and optical flanges were avoided.

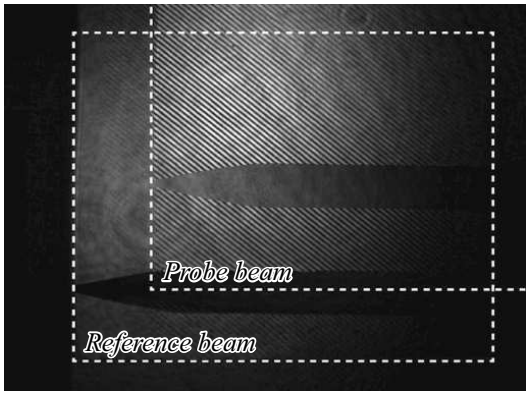

Figure 2. Interference pattern. A needle is installed in plane with the nozzle to control proper image transfer by the optical system and to calculate the image transfer scale ratio.

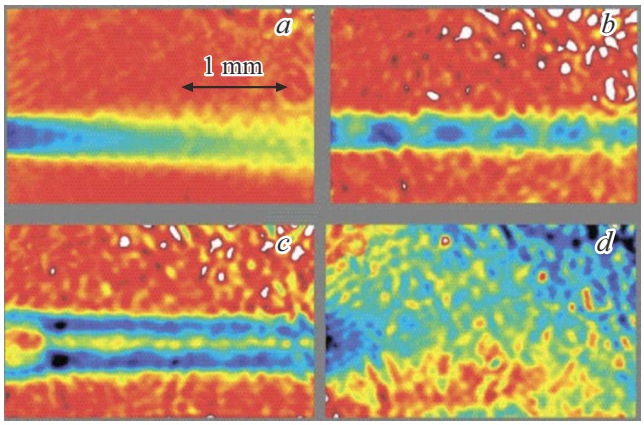

Figure 3. Phase incursion distributions for the argon jet admitted into the volume with background pressure: a — 760, b — 300, c — 100, d — 0.1 Torr.

Figure 2 shows one of the interference patterns. A needle is installed in plane with the jet to control proper image transfer by the optical system and to calculate the image transfer scale ratio (the needle thickness in its wide part was 600 μm). Then the following interference pattern processing was performed as also described in [17].

A useful area with good visibility of the fringe pattern and a priori containing the test object (gas jet) was defined on the interference pattern frame, the remaining part of the photograph discarded by applying a mask that set the signal in this area to zero. Then using the forward Fourier transform, a two-dimensional spectrum of the test interference pattern was obtained, where the bandwidth carrier peak and its vicinity were outlined by applying the spectral filter. Using the inverse Fourier transform and removing the discontinuities and slopes in the phase of the obtained signal, an additional phase incursion was restored in the object location due to the increase in the optical path directly owing to the presence of the gas target and to a somewhat different phase incursion caused by different path lengths of the probe and reference beams. The latter difference is removed by subtraction of the phase incursion with a gas jet and phase incursion without a gas jet obtained by means of identical processing of the background (without a gas jet) interference pattern. Thus, the true phase incursion associated only with the optical path variation due to the gas jet flowing through the nozzle was restored.

Figure 3 shows distributions of the phase incursion created by the argon jet (pressure in the admission line — 1 bar) admitted through the gas target nozzle with an inlet diameter of 300 μm. The gas admission system pressure was measured using the pressure gauge on the regulator of the gas cylinder used for gas admission. Zero corresponded to atmospheric pressure, thus, 1 bar corresponded to 1 atm gauge in the admission line. Gas was fed to the target from the regulator via the 6 mm tube. In this case, the target consisted of a piece of stainless steel foil 300 μm in

thickness and the same opening diameter in it. The admitted gas temperature was equal to room temperature.

At a background pressure of 760 Torr (Figure 3, *a*), a continuous jet is observed. As the distance from the nozzle grows, the phase peak value decreases. The typical (maximum) phase incursion is equal to 0.2 rad. When the background pressure is 300 Torr (Figure 3, *b*), the jet is interrupted along the longitudinal coordinate. The peak values are almost 2 times as high as in case when the background pressure is equal to atmospheric pressure. When the background pressure is equal to 100 Torr (Figure 3, *c*), the jet is broadened and doubled (has a dip in the center). Near the nozzle, there is an axisymmetric structure with a phase dip almost to the background values. The peak phase incursion values are a little higher that for the background pressure equal to atmospheric pressure. When the background pressure is at the prevacuum level (0.1 Torr, Figure 3, *d*, with continuous evacuation), it can be seen that no jet structure is observed any longer, the gas is admitted almost to the whole semispace, into the solid angle about 2π.

A similar situation was also observed for other targets. Figure 4 shows the example of distribution of the phase incursion induced by the argon jet admitted through the gas target nozzle for two background gas pressures — 520 (Figure 4, *a*) and 0.1 Torr (Figure 4, *b*). The target itself constituted a capillary 6 mm in length with an end outlet 80 μm in diameter. The admission line pressure according to the regulator pressure gauge was equal to 2 bar gauge.

At 520 Torr, formation of a gas jet with a small flare angle is observed, the gas jet center line does not coincide with the target center line. The nozzle exit was likely inclined with respect to the target. At 0.1 Torr, gas jet disintegration is observed, however, the drop of neutral atom concentration occurs not right away, but at a distance of about 0.5 mm from the nozzle exit where a phase incursion different from the background one is still observed. Though, of course, as shown in Figure 4, the main drop of the phase incursion is observed at a shorter distance from the outlet exit that is close to 100 μm, i.e. comparable with the target outlet diameter.

Summing up this chapter, it should be noted that all experiments using the prepared interferometer showed the minimum phase incursion threshold (when a difference from background noise was observed) equal to 0.03 rad, which is not bad for so-called „mass“ measurements (see, for example, [18], Ch. 7).

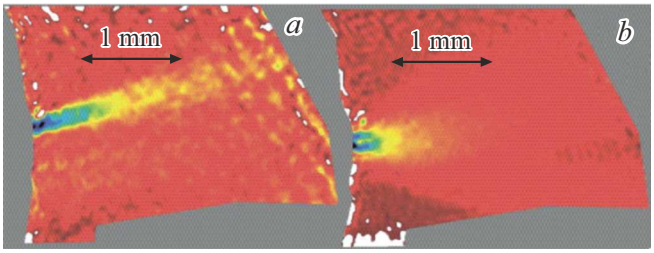

Figure 4. View of the phase incursion of gas jets emitted by the target with an outlet diameter of 80 μm at different background pressures. The admission line pressure — 2 bar (argon): *a* — background pressure 520 Torr; *b* — background pressure 0.1 Torr.

It is also interesting to assess the correlation between the phase incursion and atom density in the jet. Due to relatively low density of substance and the necessity to separate the contributions of heavy particles to the refraction (refraction index), the gas refraction index may be written as

$$n \approx 1 + 2\pi(\Sigma\chi_j N_j). \qquad (1)$$

The second term herein includes the refraction from heavy particles (atoms, molecules). Neutral gas consists of the various kinds of particles N_j with polarizabilities χ_j. Equation (1) was obtained in the following conditions: the probe radiation frequency ω is beyond the resonance with optical transition ($|\omega - \omega_{ik}| \gg \Delta\omega_{ik}$, where $\Delta\omega_{ik}$ is the transition line width. The main portion of the contribution made by heavy particles to the refraction is defined by the particles in ground electron states $i = 1$. Since the resonance transition frequencies are usually within the vacuum violet spectral band (consider important exclusions such as, for example, alkaline atoms, molecular radicals [18]) and probing is performed by visible light, then $\lambda \gg \lambda_{1k}$. With this additional condition, the polarizabilities and refraction indices are calculated using the Cauchy equations:

$$x = a + b/\lambda^2, \quad n - 1 = (A + B/\lambda^2)N/N_L, \qquad (2)$$

where $N_L = 2.7 \cdot 10^{19}\,\mathrm{cm}^{-3}$ is the Loschmidt number. The values of a and b as well as A, B (for normal conditions) for nonexcited particles of some gases are given, for example, in [18]. For argon, A is approximately equal to $3 \cdot 10^{-4}$. For the visible band, the dependence of polarizability and refraction index on the wavelength is weak, $a \gg b/\lambda^2$, $A \gg B/\lambda^2$. Neglecting this dependence and assuming the linear correlation of the polarizability and refraction from the density of particles (the Gladstone–Dahl law), the following can be written (for particles of one kind)

$$n - 1 \approx 2\pi\gamma N, \qquad (3)$$

where $\chi = A/2\pi N_L$.

Thus, the phase incursion defined as $(n-1)L2\pi/\lambda$ may be written as

$$\Delta\varphi \approx (A/N_L)NL2\pi/\lambda, \qquad (4)$$

where L is the typical transverse dimension of the object (jet) where the phase incursion occurs. Certainly, for better accuracy, such type of transverse particle distribution in the jet shall be expected, for example, azimuthal symmetry, that will make it possible to use the inverse Abelian transform to restore the real transverse particle profile in the jet, but for rough estimate assume L as the mean jet size equal (for the case in Figure 3) to the nozzle opening diameter — 300 μm. Then the phase incursion of 1 rad approximately corresponds to (accorsing to (4)) the concentration equal to N_L, i.e. the number of atoms in standing-wave gas

at atmospheric pressure and room temperature. I.e. the maximum observed phase incursion of 0.3 rad corresponds to the particle concentration of $8 \cdot 10^{18}\,\mathrm{cm}^{-3}$. Whereas the sensitivity threshold corresponds to a concentration that is an order of magnitude lower.

Conclusion

The interferometry method was used to perform experimental investigation of various gas targets for a point plasma source based on a non-uniform gas flux discharge. It was demonstrated that at considerable reduction of background gas pressure, actual jet breakdown occurred and gas was uniformly admitted in all directions. Nevertheless, the view of interference patterns (and the maximum phase incursion) suggests that even at a background pressure equal to fractions of Torr a situation takes place when a concentration of neutral gas atoms of $10^{17}-10^{18}\,\mathrm{cm}^{-3}$ may be achieved at a relatively long distance from the nozzle exit. This concentration is sufficient to ensure the electron concentration of $10^{18}\,\mathrm{cm}^{-3}$ in the plasma generated in the point discharge, which is the best result in terms of EUV and XUV radiation generation.

It should be also noted that, notwithstanding the foregoing, the point discharge is ignited easily enough in the non-uniform gas flux with longitudinal introduction of the heating radiation with respect to the jet direction as it was, for example, in the experiments described in [13]. In this case, the heating electromagnetic radiation will certainly „find “ the desired area with the required gas density, even if it is located immediately at the nozzle exit.

In case of transverse introduction of the heating radiation as in the experiments with point discharge generated in the non-uniform gas flux by the free-electron laser light [15], the electromagnetic wave beam focus cannot be placed as close as possible to the gas target nozzle. In this case, the density of neutral particles in the focus area may be insufficient to achieve the best plasma density or even insufficient for gas breakdown and discharge ignition, which is even worse. In this case, a way to increase the working gas density in the jet shall be sought for in case of admission into the reduced atmosphere. Employment of a so-called two-stream target is one of such methods [19].

This target consists of two concentric nozzles to which gases at various pressures may be supplied independently. Simultaneously, the working heavy inert gas (argon/krypton/xenon) is fed through the central nozzle. And light helium is fed to the peripheral nozzle. The presence of helium makes it possible to narrow the central heavy inert gas jet and to increase its density in the jet, other things being equal. Currently, the prototype of such target has been already made: it consists of two concentric nozzles with diameters of 0.27 mm and 0.69 mm, respectively. Gas flow rate was measured at various pressures in the admission lines of both nozzles. Experiments are being prepared to investigate the processes of jet formation by the two-stream target using the interferometric measurements. And it should be noted that constants A (see equation (2)) for heavy inert gases differ by almost an order of magnitude from that for helium. This makes it possible to rely on the fact that the heavy inert gas jet will be clearly visible against the background of the helium jet in the fringe pattern.

Funding

This study was supported by grant № 19-72-20166 provided by the Russian Science Foundation.

Conflict of interest

The authors declare that they have no conflict of interest.

References

[1] H.J. Levinson. *Proc. Int. Workshop on EUV Lithography* (CXRO, LBNL, Berkeley, CA, USA. June 13–16, 2016), p. 1. https://www.euvlitho.com/2016/P1.pdf
[2] V.M. Borisov, G.N. Borisova, A.Yu. Vinokhodov, S.V. Zakharov, A.S. Ivanov, Yu.B. Kiryukhin, V.A. Mishchenko, A.V. Prokof'ev, O.B. Khristoforov. Quant. Electron., **40** (8), 720 (2010). DOI: 10.1070/QE2010v040n08ABEH014369
[3] B. Jiang, Ch. Feng, Ch. Li, Zh. Bai, W. Wan, D. Xiang, Q. Gu, K. Wang, Q. Zhang, D. Huang, S. Chen. Scientif. Reports, **12**, 3325 (2022). DOI: 10.1038/s41598-022-07323-z
[4] N.I. Chkhalo, N.N. Salashchenko. AIP Advances, **3**, 082130 (2013). DOI: 10.1063/1.4820354
[5] H. Fiedorowicz, A. Bartnik, Z. Patron, P. Parys. Appl. Phys. Lett., **62**, 2778 (1993).
[6] S.A. Bogachev, N.I. Chkhalo, S.V. Kuzin, D.E. Pariev, V.N. Polkovnikov, N.N. Salashchenko, S.V. Shestov, S.Y. Zuev. Appl. Optics, **55**, 2126 (2016). DOI: 10.1364/AO.55.002126
[7] N.I. Chkhalo, S.A. Garakhin, A.Ya. Lopatin, A.N. Nechay, A.E. Pestov, V.N. Polkovnikov, N.N. Salashchenko, N.N. Tsybin, S.Yu. Zuev. AIP Advances, **8**, 105003 (2018). DOI: 10.1063/1.5048288
[8] S.G. Kalmykov, P.S. Butorin, M.E. Sasin. J. Appl. Phys., **126**, 103301 (2019). DOI: 10.1063/1.5115785
[9] V.Y. Banine, K.N. Koshelev, G.H.P.M. Swinkels. J. Phys. D: Appl. Phys., **44**, 253001 (2011). DOI: 10.1088/0022-3727/44/25/253001
[10] A.V. Sidorov. J. Phys. D: Appl. Phys., **55**, 293001 (2022). DOI: 10.1088/1361-6463/ac5556
[11] I.S. Abramov, E.D. Gospodchikov, A.G. Shalashov. Phys. Rev. Appl., **10**, 034065 (2018). DOI: 10.1103/PhysRevApplied.10.034065
[12] A. Shalashov, E. Gospodchikov. IEEE Trans. Antennas Propag., **64**, 3960 (2016). DOI: 10.1109/TAP.2016.2583487
[13] A.G. Shalashov, A.V. Vodopyanov, I.S. Abramov, A.V. Sidorov, E.D. Gospodchikov, S.V. Razin, N.I. Chkhalo, N.N. Salashchenko, M.Yu. Glyavin, S.V. Golubev. Appl. Phys. Lett., **113**, 153502 (2018). DOI: 10.1063/1.5049126
[14] Yu.K. Kalynov, S.V. Razin, A.V. Sidorov, A.V. Vodopyanov, A.P. Veselov. *Proc. SPIE 11582, Fourth International Conference on Terahertz and Microwave Radiation: Generation, Detection, and Applications* (Tomsk, Russia, 24–26 August 2020), **11582**, 115820P (2020). DOI: 10.1117/12.2580161

[15] V.V. Kubarev, Ya.I. Gorbachev, O.A. Shevchenko, A.V. Vodopyanov, A.V. Sidorov, A.P. Veselov. Plasma Sourc. Sci. Technol., **32**, 055004 (2023). DOI: 10.1088/1361-6595/accca9
[16] P.S. Butorin, S.G. Kalmykov, M.E. Sasin. Tech. Phys. Lett., **44** (12), 1100 (2018). DOI: 10.1134/S1063785018120209
[17] T. Barmashova, A. Luchinin, A. Murzanev, S. Razin, A. Sidorov, A. Stepanov, A. Veselov, A. Vodopyanov. IEEE Trans. Terahertz Sci. Technol., **13**, 3–9 (2023). DOI: 10.1109/TTHZ.2022.3164546
[18] V.N. Ochkin. *Spectroscopy of Low Temperature Plasma* (Wiley-VCH, Berlin, 2009)
[19] R. Rakowski, A. Bartnik, H. Fiedorowicz, F. de Gaufridy de Dortan, R. Jarocki, J. Kostecki, J. Mikołajczyk, L. Ryc', M. Szczurek, P. Wachulak. Appl. Phys. B, **101**, 773 (2010). DOI: 10.1007/s00340-010-4327-9

Translated by E.Ilinskaya